

Truth-Table Net: A New Convolutional Architecture Encodable By Design Into SAT Formulas

Adrien Benamira,¹ Thomas Peyrin,¹ Bryan Hooi Kuen-Yew²

¹ Nanyang Technological University

² National University of Singapore

adrien002@e.ntu.edu.sg, thomas.peyrin@ntu.edu.sg, dcsbhk@nus.edu.sg

Abstract

With the expanding role of neural networks, the need for complete and sound verification of their property has become critical. In the recent years, it was established that Binary Neural Networks (BNNs) have an equivalent representation in Boolean logic and can be formally analyzed using logical reasoning tools such as SAT solvers. However, to date, only BNNs can be transformed into a SAT formula. In this work, we introduce Truth Table Deep Convolutional Neural Networks (TTnets), a new family of SAT-encodable models featuring for the first time real-valued weights. Furthermore, it admits, by construction, some valuable conversion features including post-tuning and tractability in the robustness verification setting. The latter property leads to a more compact SAT symbolic encoding than BNNs. This enables the use of general SAT solvers, making property verification easier. We demonstrate the value of TTnets regarding the formal robustness property: TTnets outperform the verified accuracy of all BNNs with a comparable computation time. More generally, they represent a relevant trade-off between all known complete verification methods: TTnets achieve high verified accuracy with fast verification time, being complete with no timeouts. We are exploring here a proof of concept of TTnets for a very important application (complete verification of robustness) and we believe this novel real-valued network constitutes a practical response to the rising need for functional formal verification. We postulate that TTnets can apply to various CNN-based architectures and be extended to other properties such as fairness, fault attack and exact rule extraction.

1 Introduction

Deep Neural Network (DNN) systems offer exceptional performance in a variety of difficult domains (Goodfellow, Bengio, and Courville 2016) and today these results far outstrip our ability to secure and analyze those DNNs. As DNNs are becoming widely integrated in a variety of applications, several concerns have emerged: lack of robustness emphasized by a lack of explainability, difficulty of integrating human knowledge in post-processing and impossibility to formally verify their behavior due to their large complexity. Under these circumstances and especially when these systems are deployed in applications where safety and security are critical, the formal verification of DNN systems is under intense research efforts. For example, Tesla has recently filed

a patent on the DNNs' portability on a platform incorporating a component dedicated to formal verification (Driscoll 2020) and the EU's general data protection regulation includes a provision on AI explainability (Regulation 2016).

So far, the DNNs architectures proposed by the community have generally been evolving towards increasing performance (Vaswani et al. 2017; Brown et al. 2020; Dosovitskiy et al. 2020). Improving performance is obviously desirable, however the resulting architectures are currently very hard to verify because of their intrinsic complexity. We propose here a novel architecture that is, by design, readily verifiable.

As application, we study Deep Convolutional Neural Networks (DCNNs) from the standpoint of their complete and sound formal verification: in other words, knowing a certain property, we want to confirm whether this property holds or not for a specific DNN. DNNs complete and sound verification property methods are mainly based either on Satisfiability Modulo Theory (SMT) (Katz et al. 2017) or Mixed-Integer Programming (MIP) (Xiao et al. 2019) which are not yet scalable to real-valued DNNs. Some recent publications (Jia and Rinard 2020; Narodytska et al. 2019b, 2018) approached the problem of complete verification from the well-known Boolean SATisifiability (SAT) (Biere, Heule, and van Maaren 2009) point of view where BNNs (Hubara et al. 2016) are first converted into SAT formulas and then formally verified using SAT. This pipeline is computationally efficient (Jia and Rinard 2020), enables security verification (Baluta et al. 2019) and more generally can answer a large range of questions including how many adversarial attacks exist for a given BNN, image and noise level (Narodytska et al. 2019a). However, to date, only BNNs can be transformed into a SAT formula and, as they were not designed for this application, their corresponding SAT conversion method intrinsically leads to formulas with a large number of variables and clauses, impeding formal verification scalability. In (Jia and Rinard 2020), the authors developed their SAT solver to achieve verification scaling.

A well-known example of property to verify on image classification datasets is the robustness to adversarial attacks. The performance of formal DNN robustness verification methods is evaluated against two main characteristics: verified accuracy (i.e. the ratio of images that are correctly predicted and that do not have any adversarial attacks) and verification time (i.e. the duration to verify that one cor-

rectly predicted image in the test set does/does not have an adversarial attack). The verification time is the sum of the problem construction time and its resolution time. The latter is intimately related to the quality of the solver and the complexity of the DNN encoding: a less efficient encoding and the solver will lead to a longer time to verify an image. Most robustness improvements in the literature have been in the form of new trainings (Carlini et al. 2017; Wong and Kolter 2018; Wong et al. 2018; Dvijotham et al. 2018; Raghunathan, Steinhardt, and Liang 2018; Mirman, Gehr, and Vechev 2018), new testing method to increase robustness (Carlini et al. 2017; Sahoo et al. 2020; Dvijotham et al. 2018), new certification method to guarantee robustness properties (Sahoo et al. 2020; Wong and Kolter 2018; Wong et al. 2018; Dvijotham et al. 2018) or new formal verification methods (Ehlers 2017; Lomuscio and Maganti 2017; Cheng, Nürenberg, and Ruess 2017; Mirman, Gehr, and Vechev 2018; Shih, Darwiche, and Choi 2019; Wu et al. 2022; Lomuscio, Qu, and Raimondi 2017).

Our contributions. We describe in this work a new architecture, encodable **by construction** into SAT formulas. It therefore comes as a complement to these previous approaches (our architecture can for example be trained with a certification method to further increase robustness). In addition, while we focus on the well-studied robustness to adversarial attacks property, our novel architecture generally allows a more compact symbolic encoding, leading to networks that are more amenable to verify most properties. In this work, we essentially offer three main contributions:

1. We define a new family of real-valued DCNNs that can be compactly encoded into SAT formulas: Truth Table Deep Convolutional Neural Network (**TTnet**). Our TTnet simplifies its 2D-CNN filter formulation in the form of a truth table to allow weights and certain intermediate values to be real. To the best of our knowledge, this is the first method to encode a real-valued DCNN into SAT, while achieving sufficient natural accuracy for practical use.

2. We show that TTnets offer two main valuable conversion properties over BNNs:

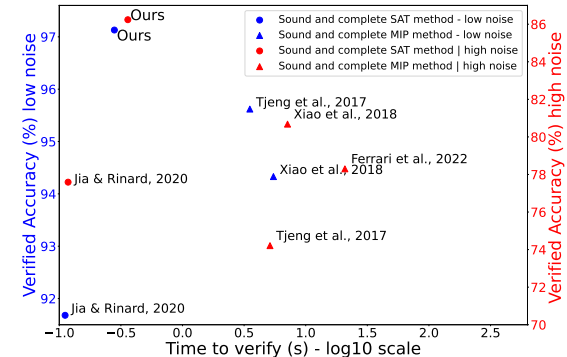
(2-a: Post-tuning) The first one allows us to integrate human knowledge in the post-processing: we can manually modify a DCNN filter activation towards a desired goal. For example, we decided to focus on reducing overfitting and, to this end, we characterize TTnet logic rules resulting from overfitting and propose a filtering approach. The latter increases the verified accuracy without decreasing the natural accuracy: +0.43% and +0.29% for high noise MNIST and CIFAR-10 respectively.

(2-b: Tractability) The second property enables to compute all possible model inputs/outputs prior to deployment in production. In an adversarial setting, we can assess whether the input noise will propagate to the output. We can therefore disregard filters with no impact on the output. This leads to a lower number of clauses and variables in the SAT formulas compared to BNNs, thus enabling the usage of generic SAT solver. Comparing to the BNN/SAT method, our SAT formulas are 5 and 9 times more compact for clauses number for high noise MNIST and CIFAR-10 respectively.

3. We apply our model to **complete robustness verification**. Our new TTnet model is the first complete and sound verification method allowing real-valued weights with competitive speed and no timeout. Besides, focusing on the robustness property, TTnet improves the verified accuracy over all BNN-based methods and more generally proposes a competitive trade-off between verified accuracy and verification time over all complete verification methods (Xiao et al. 2019; Tjeng, Xiao, and Tedrake 2019; Jia and Rinard 2020; Narodytska et al. 2019b; Ferrari et al. 2022; De Palma et al. 2022). A comparison of our approach with the state-of-the-art methods for MNIST with low ($\epsilon = 0.1$)/high ($\epsilon = 0.3$) l_∞ noise perturbation is given in Figure 1. On MNIST we can observe that with 97.12% and 86.24% respectively, we outperform previous best verified accuracy from ICLR 2019 (Tjeng, Xiao, and Tedrake 2019; Xiao et al. 2019) that reached 95.62% and 80.68% respectively, in addition to a shorter verification time. We highlight that our goal is to propose a competitor to BNN for SAT complete formal verification (using robustness as example property), not to propose a competitive robustness method.

We also show that our model can scale to ImageNET. Finally, as robustness is merely one example property that our model can verify, we argue that TTnet has the potential to be competitive on many other strategic properties.

Figure 1: Comparison of complete SAT and MIP methods for MNIST low noise ($\epsilon = 0.1$, in blue) and high noise ($\epsilon = 0.3$, in red) with regards to verified accuracy and verification time. Our method is more accurate than all methods and faster than the sound+complete MIP (triangle points).



Outline. Section 2 introduces notations and related work. Section 3 presents our TTnet model and its two main properties. Section 4 details the complete robustness verification set-up and reports the evaluation results. Finally, we present TTnet’s limitations in Section 5 and conclude in Section 6.

2 Related work and background

Boolean SATisifiability. The SAT problem (Biere, Heule, and van Maaren 2009) is that of deciding whether there exists a variable assignment to satisfy a given Boolean expression Φ . We can consider a Boolean expression in a Conjunctive Normal Form (CNF) or in a Disjunctive Normal Form

Table 1: Comparison of state-of-the-art formal verification methods according to four criteria: the method type (sound and complete), the method applicability scope (can the method extend to all properties and all DNNs), the solver used and the method scalability.

Method	Type		Applicability scope		Solver Used	Scalability	
	Sound	Complete	All	All		MNIST	
			Properties	DNNs		Low / High	CIFAR-10
(Jia and Rinard 2020)	✓	✓	✓	only BNN	general SAT	✓	✓
(Narodytska et al. 2019a)	✓	✓	✓	only BNN	specific SAT	only t_p	✗
(Xiao et al. 2019)	✓	✓	✓	✓	MIP	✓	✓
(Tjeng, Xiao, and Tedrake 2019)	✓	✓	✓	✓	MIP	✓	✓
(Miller et al. 2022)	✓	✗	✗	✗	MIP	✓	✓
(Wang et al. 2021a)	✓	✗	✗	✗	MIP	✓	✓
(Xu et al. 2020a)	✓	✗	✗	✗	-	✗	✗
(Zhang et al. 2021a)	✓	✗	✗	✗	-	✓	✓
(Zhang et al. 2019)	✓	✗	✗	✗	-	✓	✓
(Andriushchenko and Hein 2019)	✓	✓	✗	only dec. tree	-	✗	✓
(Kurtz and Bah 2021)	✓	✓	✗	only BNN	MIP	✗	✗
(Jia and Rinard 2021b)	✓	✓	✓	✓	MIP	✗	✗
(Zhang et al. 2021b)	✓	✓	✓	only BNN	MIP*	✓	✗
Ours	✗	✓	✓	only TTnet	general SAT	✓	✓

*Probabilistic solver.

(DNF). They are both defined over a set of Boolean variables (x_1, \dots, x_n) . A literal l_i is defined as a variable x_i or its complement \bar{x}_i . A CNF is a conjunction of a set of clauses: $\Phi = (c_1 \wedge \dots \wedge c_m)$, where each clause c_j is a disjunction of some literals $c_j = l_{j1} \vee \dots \vee l_{jr}$. A DNF is a disjunction of a set of clauses: $\Phi = (c_1 \vee \dots \vee c_m)$, where each clause c_j is a conjunction of some literals $c_j = l_{j1} \wedge \dots \wedge l_{jr}$. A pseudo-Boolean constraint has the form: $\sum_{p=1}^N a_p l_p \circ b$, where $a_p \in \mathbb{Z}$, $b \in \mathbb{Z}$ and $\circ \in \{\leq, =, \geq\}$, which can be mapped to a SAT formula (Roussel and Manquinho 2009). However, such a conversion generally leads to a tremendous number of clauses and literals compared to the number of variables in the original pseudo-Boolean form, making it impractical to comprehend. For an illustration of the latter, see Appendix B with examples of inequality conversion into SAT formulas according to different methodologies.

SAT encoding of neural networks. The sole published method converting a DNN into a SAT formula is limited to BNNs (Narodytska et al. 2018; Cheng et al. 2018) and involves recomposing a block formed of a Two-Dimensional Convolutional Neural Network (2D-CNN) layer, a batch normalization layer and a step function into an inequality in order to apply the pseudo-Boolean constraint (Roussel and Manquinho 2009). This approach has been further refined using a different training method and a specific SAT solver, resulting in a significantly reduced verification time (Jia and Rinard 2020). Although the proposed inequality rewriting is elegant, the corresponding SAT formula still contains a large number of clauses and literals compared to the number of variables in the pseudo-Boolean constraint. This prevents the tractability of those SAT/BNNs formulas. In this work, we will only focus on comparison with DNN models, and not other machine learning family such as (Andriushchenko and Hein 2019). The main feature of DNNs is that there are more parameters in the model than samples in the dataset. This is not the case with decision trees. Their learning capacity is very different and for example, we are able to learn on ImageNET, in contrary to them.

Sound, complete verification and robustness. We provide in Appendix A the definition of completeness, sound-

ness, etc. Complete and sound property verification of SAT-convertible DNNs has been presented in (Narodytska et al. 2018) as follows: given a precondition $prec$ on the inputs x , a property $prop$ on the outputs o and a SAT relations given by a DNN between inputs/outputs denoted as $DNN(x, o)$, we check whether the following statement is valid: $prec(x) \wedge DNN(x, o) \implies prop(o)$. In order to seek a counter-example to this property, we look for a satisfying assignment of $prec(x) \wedge DNN(x, o) \wedge \neg prop(o)$. An application example of property verification is to check for the existence of an adversarial perturbation in a trained DNN. In this case, $prec$ defines an ϵ -ball of valid perturbations around the original image and $prop$ states that the classification should not change under these small perturbations. Therefore, we distinguish the traditional "natural accuracy" from the "verified accuracy", the latter measuring the fraction of the predictions which remains correct for all adversarial attacks within the perturbation constraints. Table 1 presents a comparison of the functionalities of current state-of-the-art sound and complete verification methods. **In this work, our goal is not to propose a new state-of-the-art formal method dedicated to robustness, but to propose a new architecture that can scale and be used for any formal complete and sound property verification.** We then apply it to robustness against adversarial attack, a well studied property. Therefore, we compare our work to complete and sound methods that can be used for most properties: (Jia and Rinard 2020; Narodytska et al. 2019a; Xiao et al. 2019; Tjeng, Xiao, and Tedrake 2019; Ferrari et al. 2022; De Palma et al. 2022). We also highlight that verification methods (Singh et al. 2019b,a; Wang et al. 2021b; Zhang et al. 2019) are sound but incomplete. Finally, the work (Jia and Rinard 2021a) shows that floating-point MIP verification methods can be unsound in some specific case. For a more detailed state-of-the-art, we refer to (Huan et al. 2022).

Two-dimensional Convolutional Neural Networks. A Boolean function has the form $\{0, 1\}^n \rightarrow \{0, 1\}$ and its corresponding truth table lists the outputs for all 2^n possible inputs combinations (easily set up when n is not too large). Within our method, we consider the 2D-CNN as a Boolean function $\Phi_{(f, s, p, k, c)}$ which, for a given filter f , takes $n = k^2 c / g$ inputs at position (i, j) with k the kernel size, c the number of input channels, s the stride, p the padding and g the group parameter (Dumoulin and Visin 2016). The outputs can be written as $y_f^{(i,j)} = \Phi_f(x_1^{(i,j)}, \dots, x_n^{(i,j)})$. If we now consider a multi-layer network, a similar truth table can be constructed, except for the kernel size k that needs to be replaced by a *patch function*, sometimes also referred to as the size of a receptive field (Araujo, Norris, and Sim 2019). We denote the vector obtained after the flatten operation and before the final classifier layer as the vector of features V .

3 Truth Table Deep Convolution Neural Network (TTnet)

In an attempt to address the drawbacks of the high encoding complexity of the SAT formulas obtained from BNN's transformation process, we designed a new DNN architec-

ture that admits a more compact symbolic encoding. We use real-weighted convolutions and aggregations that are further binarized with step-functions. These convolutions can be fully represented with truth tables, as long as the number of inputs in the filter is low-dimensional.

Figure 2 outlines the architecture of the TTnet model. In order to explain our model, we will initially analyse a 2D-CNN layer with a single filter (Section 3.1). Next, we will define the Learning Truth Table (LTT) block of our TTnet architecture (Section 3.2). Finally, Sections 3.3 and 3.4 present the whole architecture of the TTNet and its main results, respectively. We provide a companion video <https://youtu.be/loGlpVcy0AI>.

3.1 SAT encoding of a one-layer 2D-CNN

For this first building block, we consider as input a binary image with one channel and as a model a trained DCNN with only one layer. We first start to encode one filter, then we will increase the complexity of our model by adding more filters to the 2D-CNN and then channels to the inputs.

One filter. The main idea is to fix the number of possible outputs of the 2D-CNN by fixing the number of its possible inputs, which will allow us to later test all possible combinations. Following notations introduced in Section 2, we have as output $y_{binary,f}^{(i,j)}$ for filter f and n number of inputs:

$$y_{binary,f}^{(i,j)} = \text{Bin}(y_f^{(i,j)}) = \text{Bin}(\Phi_f(x_1^{(i,j)}, \dots, x_n^{(i,j)})) \quad (1)$$

with Bin being the Heaviside step function, defined as $\text{Bin}(x) = \frac{1}{2} + \frac{\text{sgn}(x)}{2}$. If $x_j \in \{0, 1\}$, we can establish the truth table of the 2D-CNN’s filter f by trying all the possible inputs, for a total of 2^n operations. In this paper, we will limit ourselves to $n \leq 9$ (unless stated otherwise). Hence, with $2^9 = 512$ operations, we can trivially generate our truth table. Then, we can convert the truth table into a simplified SAT formula and by doing so we can rewrite Equation 1 as:

$$y_{binary,f}^{(i,j)} = \text{SAT}_f^{\text{DNF}}(x_1^{(i,j)}, \dots, x_n^{(i,j)}) = \text{SAT}_f^{\text{CNF}}(x_1^{(i,j)}, \dots, x_n^{(i,j)})$$

with $\text{SAT}_f^{\text{DNF}}$ (resp. $\text{SAT}_f^{\text{CNF}}$) being the formal expression of the filter in the DNF form (resp. CNF form). It is noteworthy that unlike previous works, our approach is not limited to binary weights but allows for arbitrary weights within the 2D-CNN. Example 1 illustrates the described construction.

Example 1. We consider a 2D-CNN with one filter and a kernel size of 2, with the weights:

$$W_1 = \begin{bmatrix} 10 & -1 \\ 3 & -5 \end{bmatrix}. \text{ As } c = 1, \text{ we have } X = \begin{bmatrix} x_0 & x_1 \\ x_2 & x_3 \end{bmatrix}$$

and the sixteen possible entries are: $\begin{bmatrix} 0 & 0 \\ 0 & 0 \end{bmatrix}, \begin{bmatrix} 0 & 0 \\ 1 & 0 \end{bmatrix}, \begin{bmatrix} 0 & 0 \\ 1 & 1 \end{bmatrix}, \dots, \begin{bmatrix} 1 & 1 \\ 0 & 1 \end{bmatrix}, \begin{bmatrix} 1 & 1 \\ 1 & 1 \end{bmatrix}$.

For each input, we calculate the corresponding output: $y = [0, -5, 3, -2, -1, -5, 3, -2, 10, 5, 13, 8, 9, 4, 12, 7]$. After binarization with the Heaviside step function, we have $y_{binary} = [0, 0, 1, 0, 0, 0, 1, 0, 1, 1, 1, 1, 1, 1, 1, 1]$. After

simplification, we have $\text{SAT}_1^{\text{DNF}} = (x_2 \wedge \overline{x_3}) \vee x_0$ and $\text{SAT}_1^{\text{CNF}} = (x_2 \vee x_0) \wedge (\overline{x_3} \vee x_0)$ with Quine-McCluskey algorithm (Quine 1952).

Multiple filters and channels. Transposing to the case of multiple filters is straightforward: the above described method is simply repeated for each individual filter, thus yielding one expression per filter. As convolutional networks take several channels as input, the number of input variables rises substantially. For example, a 2D-CNN that takes 32 input channels with a kernel size of 2 yields an input of size 128, well above our limit set at $n = 9$. In order to overcome this effect, we group the channels using the group parameter (Dumoulin and Visin 2016). Grouped convolutions divide the input channels into g groups, then apply separate convolutions within each group; this effectively decreases the number of inputs to each individual filter by a factor of g . We have in that case $n = k^2c/g$. In the model diagram in Figure 2, the groups are separated by the horizontal dotted lines. In the previous example, by using 16 groups, the number of inputs of our truth tables becomes $\frac{32}{16} \times 2^2 = 8$.

3.2 Learning Truth Table (LTT) block

In order to improve the performance of the model, we add an amplification layer that will increase the learning capacity of the DCNN without augmenting the size of the patches seen by the DCNN (Sandler et al. 2018).

Amplification layer. In the previous subsection, we pointed out that only the 2D-CNN input size matters when establishing the 2D-CNN SAT expression. Therefore, we can add a second layer as long as we do not increase the patch size. This is achieved by adding a layer with kernel size 1. It can be noted that the intermediate values from the first layer do not need to be binary anymore. Figure 2(b) shows the architecture of the LTT block. A block is composed of two 2D-CNN layers with a so-called amplification parameter which corresponds to the ratio between the number of filters of the first layer and the number of filters of the second layer. We set the amplification parameter value at 8: you can find the extended study at Section F.

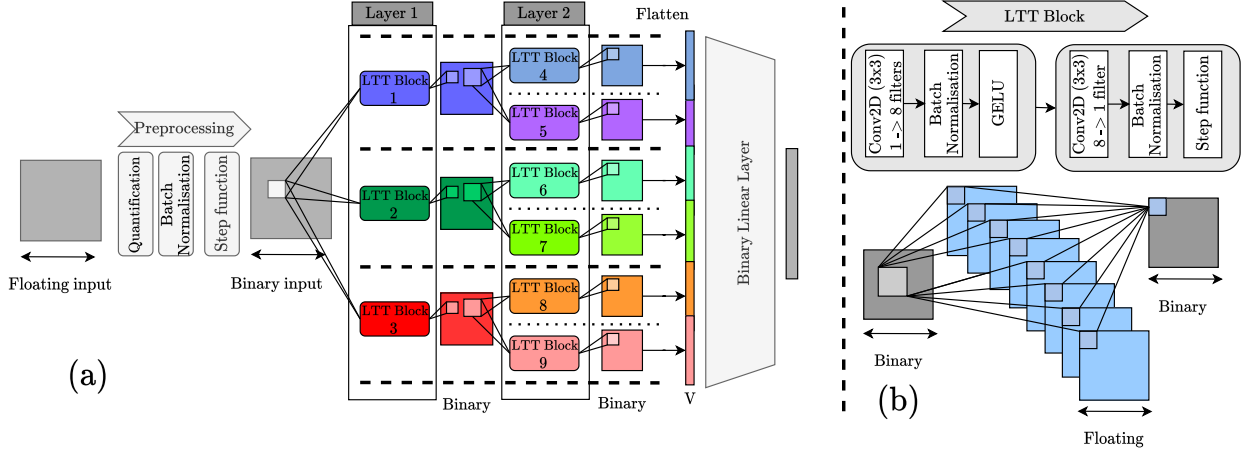
3.3 The TTnet architecture

We show in Figure 2 how the LTT block defined previously is integrated in TTNet: each LTT layer is positioned like a 2D-CNN layer except that its filters are not linear, they are expanding auto-encoders.

cc

Pre-processing layer. DCNNs inputs are usually floating points. However, encoding floating points into SAT typically implies high complexity. In order to simplify the verification process and to improve the network robustness, we applied a three-step first-layer or pre-processing procedure: (i) Quantification of inputs (Jia and Rinard 2020); (ii) Batch normalization (Narodytska et al. 2019b); and (iii) Step function. Details on the quantification step (i) are given in Appendix C.2. We highlight that our pre-processing layer is the same as (Jia and Rinard 2020).

Figure 2: (a) General architecture of the TTnet model with a one-channel input. Layer 0 is a pre-processing layer that allows image binarization. Then follow two layers of Learning Truth Table (LTT) blocks: three blocks in the first layer, six in the second. It should be noted that the LTT block of layer 2 does not take as input all the filters of layer 1, as it is usually the case: it only takes the filter of their groups. Finally, the last linear layer performs the classification. (b) Architecture of Learning Truth Table (LTT) block. A LTT block is composed of two layers of grouped 2D-CNN with an expanding factor of 8. It can be seen as an expanding auto-encoder. The intermediate values are real and the input/output values are binary.



Final layer. TTnet uses a single linear layer as a classifier block. Indeed, it is straightforward to grasp and it can be easily encoded into SAT using pseudo-Boolean constraint as detailed in Section 2 as long as the weights are integers (details of that encoding are presented in Appendix C.3).

3.4 Experiments: natural accuracy comparison

We now assess the natural accuracy performances of our TTnet architecture and compare it to existing approaches. A comparison of TTnet model features with BNN and DCNN is presented in Table 2.

Table 2: TTnet features, comparison with BNN and DCNN.

	TTnet	BNN	DCNN
Weights type	Floating	Binary	Floating
Intermediate values type	Mixed Floating/Binary	Binary	Floating
Grouped 2D-CNN	✓	✗	✗
Classifier	Linear	MLP*	MLP*

* MLP: Multi-Layer Perceptron.

Training procedure. We compare TTnet, BNN and standard real-valued DCNN. We use Model B (7,7) (Table 10 in Appendix C.1), without the amplification blocks and group parameter at one for BNN and DCNN. We believe the settings to be balanced between the models as the number of parameters to train for the BNN and DCNN is higher than for TTnet and the patch size is the same for the three models. TTnet and DCNN FLOPS are also comparable. We note that after SAT conversion, our FLOPS decreases to zero (no more float). We reproduced the exact same published training setting proposed in (Jia and Rinard 2020) for TTnet and BNN. TTnet has a final layer with integer values just for this experiment. We stopped the training at 45 epochs for all

three models to prevent overfitting. We also compare TTnet for two values of truth table sizes n : 9 and 27 (we change 9 to 27 by increasing the number of filters in one group from 1 to 3). We complete the comparison with training and testing time (see Table 11 in Appendix D).

Results for small verifiable models. The results are presented in Table 3. TTnet yields improved natural accuracy over BNN, but of course lower than the original DCNN. By increasing the truth table dimension n to 27 and by increasing the number of filters in one group from 1 to 3, the enhancement over BNN is larger while the gap is reduced with DCNN: no difference for MNIST, -8.08% for CIFAR-10.

Table 3: Comparison of natural accuracy between TTnet with two truth table sizes, BNN and DCNN.

	TTnet (n = 9)	TTnet (n = 27)	BNN	DCNN
MNIST	98.35%	98.47%	96.98%	98.49%
CIFAR-10	54.11%	58.08%	53.53%	66.16%
Number of parameters	30.8K	38.5K	44.7K	44.7K
Patch size	(7,7)	(7,7)	(7,7)	(7,7)
MFLOPs (before SAT conv.)	0.7	0.9	NA - no float	0.9
MFLOPs (after SAT conv.)	0	0	NA - no float	0.9

Results for ImageNET. As our ambition is to propose a model formally verifiable by design, we tested its scaling of our model to ImageNET dataset (Deng et al. 2009) (see Table 4), with 18 layers of TTnet, for a truth table of size $n = 48$ which remains computable. We can observe that TTnet can be adapted to ImageNET with improved accuracy over BNN’s original paper (Hubara et al. 2016) and comparable performances over XNOR-Net (Rastegari et al. 2016). We note TTnet’s satisfactory natural accuracy for practical use for real life dataset (see Appendix E for more details).

TTnets currently do not allow formal verification for ImageNET ($n = 48$ leads to difficulty in transforming into SAT), but we emphasize that no state-of-the-art complete formal verification method could scale to this dataset yet.

Table 4: Comparison of top 1 and top 5 natural accuracy between TTnet, BNN and XNOR-Net on ImageNET.

Accuracy	TTnet (n=48)	BNN (Hubara et al. 2016)	XNOR-Net (Rastegari et al. 2016)
top 1	45.9 %	27.9 %	44.2 %
top 5	69.1 %	50.4 %	69.2 %

4 Application to complete robustness verification

We now describe the two main valuable conversion properties of TTnet: post-tuning in Section 4.1 and tractability in Section 4.2. Then, we apply TTnet to complete robustness verification in Section 4.3. For fair comparison, in this section, we use the same pre-processing as in (Jia and Rinard 2020), the reference BNN paper for our comparison in Table 7 and the same quantification: 0.61 for MNIST and 0.064 for CIFAR10 for the pre-processing layer.

4.1 Post-tuning: characterizing and filtering overfitting DNF clauses

Our model gives the user the freedom to modify the set of SAT equations for all filters f . It addresses a very general problem: adding domain knowledge into a trained NN. Namely, we wish to reduce the model overfitting part in order to increase the verified accuracy without modifying the natural accuracy. To do so, we first propose a characterization of the DNF clauses responsible for the overfitting of the TTnet followed by a very simple suppression process.

As we have made the SAT clauses explicit, we may then modify them for a specific purpose. Drawing back on Example 1 of Section 3.1, we may consider, for example, that the DNF clause $(x_2 \wedge \bar{x}_3)$ is too general and thus decide to remove it from the DNF equation. By doing so, we modify the activation of filter 1 and in turn directly integrate human knowledge in post-tuning.

Characterizing overfitting DNF clauses. A DNF clause is considered as an overfitting DNF clause if the ratio of the actual number of literals over the total number of possible literals in the clause is below a certain threshold (cf Appendix D). Indeed, the intuition behind the previous heuristic is that the more literals in the DNF clause, the more constraints on the input image, which hinders the proper generalization of the model. A ratio value of 1 means that the filter is only active if the patch exactly overlaps the DNF clause. Therefore, by changing only one bit, we deactivate that filter.

Filtering out overfitting DNF clauses. Upon prescribing the overfitting threshold, tagged DNF are filtered out. Next, among the remaining DNF clauses, we tag as additional overfitting DNF clauses those having the maximum literal ratio in the formula. Finally, we apply a random Bernoulli process to partially delete tagged DNF clauses. This technique increases the verified accuracy of the TTnet models

trained on CIFAR-10: from 22.79% to 23.08%, with essentially no effect on natural accuracy (see results in Table 5).

Table 5: Effect on verified and natural accuracy of the overfitting DNF clauses filtering operation for the final model.

Dataset (noise)	Method	Accuracy	
		Verified	Natural
MNIST ($\epsilon_{test} = 0.3$)	TTnet Model B(7,7)	79.93%	96.79%
	TTnet+filtering	80.36% (+0.43%)	96.73% (-0.06%)
CIFAR-10 ($\epsilon_{test} = 8/255$)	TTnet Model A(7,7)	22.79%	31.18%
	TTnet+filtering	23.08% (+0.29%)	31.13% (-0.05%)

4.2 Tractability: computing all the possibilities of the adversarial setup before production

Another feature of the TTnet’s architecture is that one can calculate all the possible inputs/outputs of the LTT block before using the model in production. As we use small and independent truth tables, we can locally compute the noise propagation. Figure 4 in Appendix I shows the adversarial setting pipeline, how the noise is created in the pre-processing layer and how it propagates through subsequent layers. The core procedure for the conversion of TTnet into SAT is explained in Algorithms 1 and 2 in Appendix H.

Encoding pixel noise. Let us consider some noise (e.g. norm-bounded by l_∞) added to the input image prior binarization. After the pre-processing layer, a binarized pixel may either remain unchanged by the perturbation (fixed to 0 or 1), or it may flip (from 0 to 1 or from 1 to 0) and hence we consider these flipping bits as “unknown”, denoted as U .

Noise propagation at the block level. In order to encode the noise propagation through the blocks, we encode in SAT the input/output relationship through the truth table. An example is given in Figure 4 in Appendix I.

Encoding the attack at the final layer level. Ultimately, for the final layer, we encode $r_{i,j} = y_i - y_j > 0$ as a refined cardinality constraint which denotes whether the score of class i is higher than the score of class j . Being able, thanks to the truth table nature of our architecture, to distinguish between known and unknown elements of the feature V of the image allows us to reduce significantly the size of the SAT formulas when compared to state-of-the-art models.

Results. Table 6 reports the consequences of this tractability property showing a substantial improvement over previous works. For MNIST high noise, our SAT equation yields on average 4K clauses and 1K variables, while (Jia and Rinard 2020) reported 21K clauses and 48K variables and (Narodytska et al. 2019b) at least 20K clauses and 8K variables. Similar trends were observed with CIFAR-10 noise. The drastic reduction in the size of SAT formulas renders our model truly amenable to formal verification. However, this SAT filtering induces a small extra time computation.

4.3 Formal and complete robustness verification for untargeted attack

Methodology. We studied natural accuracy, verified accuracy for l_∞ -norm bounded input perturbations and veri-

Table 6: Comparison of the number of clauses and variables for a given DCNN, for different encoding. The lower the better for the first two columns.

Dataset (noise)	Method	Number of clauses	Number of variables	Natural Accuracy
MNIST ($\epsilon_{test} = 0.3$)	TTnet Model B(7,7)	4K	1K	96.79%
	BNN (Jia and Rinard 2020)	21K	48K	96.36 %
	BNN (Narodytska et al. 2019b)*	20K	8K	96.0%
CIFAR-10 ($\epsilon_{test} = 8/255$)	TTnet Model A(6,6)	1K	0.4K	31.18%
	BNN (Jia and Rinard 2020)	9K	13K	35.00%

* results given on the first 1K images of the test set.

fication time on MNIST and CIFAR-10. Again, we reproduced the exact same published training setting as proposed in (Jia and Rinard 2020), same pre-processing and quantification. We compared our work with the state-of-the-art of exact verification for BNNs (Jia and Rinard 2020; Narodytska et al. 2019b) and for real-valued networks (Xiao et al. 2019; Tjeng, Xiao, and Tedrake 2019). We report the best verification accuracy for Model A(6,6), Model B(7,7) and Model C(7,7) with $n = 9$ and with the filtering (cf Table 13 in Appendix F for extended results), and we did the same for the baselines. Experimental settings and extended comparisons are detailed in Appendix D.

Table 7: Application of TTnet to complete adversarial robustness verification for low and high noise bounded by l_∞ . We tabulate results of verified accuracy, natural accuracy and mean verification time on MNIST and CIFAR-10 datasets in comparison to state-of-the-art SAT methods. The best verified accuracy is displayed in bold.

Dataset (noise)	Complete Method	Accuracy	Verification time (s)	Timeout
		Verified	Natural	
MNIST ($\epsilon_{test} = 0.1$)	TTnet	97.12%	98.33%	0.3743
	(Jia and Rinard 2020)	91.68%	97.46%	0.1115
	(Narodytska et al. 2019b)*	20.0%	96.0 %	5
MNIST ($\epsilon_{test} = 0.3$)	TTnet	86.24%	97.43 %	0.5586
	(Jia and Rinard 2020)	77.59%	96.36%	0.1179
CIFAR-10 ($\epsilon_{test} = 2/255$)	TTnet	34.32%	49.23%	0.2886
	(Jia and Rinard 2020)	32.18%	37.75%	0.0236
CIFAR-10 ($\epsilon_{test} = 8/255$)	TTnet	23.08%	31.13%	0.3887
	(Jia and Rinard 2020)	22.55%	35.00%	0.1781

* results given on the first 1K images of the test set. Moreover the authors only authorize at maximum 20 pixels to switch.

Comparison with SAT methods. As shown in Table 7, our verified accuracy is always superior to that of the BNN. In addition, we experienced the same resolution time as BNN’s using a general SAT solver (namely MiniCard (Liffliton and Maglalang 2012)). We highlight here that in (Jia and Rinard 2020) the SAT solver is custom-made and specific to their problem, while in our case we use a general one. This point is important, indeed when using a general SAT solver, (Jia and Rinard 2020) reports for MNIST high noise a resolution time of 0.242s, where ours is 0.00079s with the same SAT solver. **We are exploring here a proof of concept of TTnets for a very important application and we believe this already justifies their potential.** We give comparisons with MIP and incomplete methods in Appendix F.3.

Comparison with MIP methods. As presented in Figure 1, we could demonstrate that TTnet verified accuracy is

higher than that of the real value-based models in all MNIST cases. We also show that, with the general SAT solver MiniCard, we experience a resolution time of one to two orders of magnitude faster than the real-valued models, despite a lower verified accuracy for CIFAR-10, cf Table 16. Moreover, TTnet presents no timeout: it always returns an answer whereas it is not the case for (Xiao et al. 2019; Ferrari et al. 2022; De Palma et al. 2022), which is a competitive advantage.

Comparison with BNN with the same architecture as TTnet. As the BNN architectures in (Jia and Rinard 2020) are different from ours, we reproduce the results for BNN with our exact same architecture and the exact same training conditions: results are presented in Table 8. We can observe that our model always outperforms the BNN model in term of natural and verified accuracy. We believe that the TTNet strength lies first in the decoupling, then in the LTT block architecture and finally in the ability to post-process them.

Table 8: BNN as TTnet ModelB(7,7) for fair comparison

Dataset (noise)	Complete Method	Accuracy		Verification time (s)	Timeout
		Verified	Natural		
MNIST ($\epsilon_{test} = 0.3$)	TTnet ModelB(7,7)	80.36%	96.43 %	0.5722	0
	BNN as ModelB(7,7)	49.53%	93.62%	0.010	0
CIFAR-10 ($\epsilon_{test} = 2/255$)	TTnet ModelB(7,7)	33.04%	40.62%	0.7782	0
	BNN as ModelB(7,7)	28.43%	37.66%	0.008	0

5 Limitation and future work

Scaling to large models. We designed a new DCNN that aimed to reduce the complexity of the network in order to increase its verification scalability. One may wonder what impact the group parameter has on the learning ability of a large network. In Table 4 we show that TTnet can scale to ImageNET with a comparable natural accuracy to XNORnet (Rastegari et al. 2016). Future works should focus on improving the natural accuracy of the model without increasing n (Liu et al. 2018; Bello et al. 2021).

Other architectures and properties. Our method can be applied to architectures that use CNNs (like Graph-CNN). On the other hand, designing truth table-based methods for non-CNN architectures (e.g. Transformers) is an interesting direction for future work. Moreover, the compactness of TTnet can be extended to other properties like fairness (Sun et al. 2021; Garg et al. 2019), bit fault attack (Hong et al. 2019; Rakin, He, and Fan 2020), privacy (Chabanne et al. 2017) and homomorphic encryption (Sanyal et al. 2018).

Global and exact rules extractions. Our method can be applied to rule extraction field as in (Wang et al. 2021b; Yang et al. 2021): in fact, TTnet allows the DNN to be written as a sum of DNF: this property can be studied in an other work for exact and global rules extractions on smaller datasets.

6 Conclusion

We proposed a novel architecture of SAT encodable real-valued DCNN based on truth tables that constitutes a practical complementary approach to the existing methods. We

believe that the TTnet constitutes a suitable approach to the rising demand for functional formal verification.

References

Abío, I.; Nieuwenhuis, R.; Oliveras, A.; and Rodríguez-Carbonell, E. 2011. BDDs for pseudo-Boolean constraints—revisited. In *International Conference on Theory and Applications of Satisfiability Testing*, 61–75. Springer.

Andriushchenko, M.; and Hein, M. 2019. Provably robust boosted decision stumps and trees against adversarial attacks. *Advances in Neural Information Processing Systems*, 32.

Araujo, A.; Norris, W.; and Sim, J. 2019. Computing Receptive Fields of Convolutional Neural Networks. *Distill*. <Https://distill.pub/2019/computing-receptive-fields>.

Baluta, T.; Shen, S.; Shinde, S.; Meel, K. S.; and Saxena, P. 2019. Quantitative verification of neural networks and its security applications. In *Proceedings of the 2019 ACM SIGSAC Conference on Computer and Communications Security*, 1249–1264.

Bello, I.; Fedus, W.; Du, X.; Cubuk, E. D.; Srinivas, A.; Lin, T.-Y.; Shlens, J.; and Zoph, B. 2021. Revisiting resnets: Improved training and scaling strategies. *arXiv preprint arXiv:2103.07579*.

Biere, A.; Heule, M.; and van Maaren, H. 2009. *Handbook of satisfiability*, volume 185. IOS press.

Brown, T. B.; Mann, B.; Ryder, N.; Subbiah, M.; Kaplan, J.; Dhariwal, P.; Neelakantan, A.; Shyam, P.; Sastry, G.; Askell, A.; et al. 2020. Language models are few-shot learners. *arXiv preprint arXiv:2005.14165*.

Carlini, N.; Athalye, A.; Papernot, N.; Brendel, W.; Rauber, J.; Tsipras, D.; Goodfellow, I.; Madry, A.; and Kurakin, A. 2019. On evaluating adversarial robustness. *arXiv preprint arXiv:1902.06705*.

Carlini, N.; Katz, G.; Barrett, C.; and Dill, D. L. 2017. Provably minimally-distorted adversarial examples. *arXiv preprint arXiv:1709.10207*.

Chabanne, H.; De Wargny, A.; Milgram, J.; Morel, C.; and Prouff, E. 2017. Privacy-preserving classification on deep neural network. *Cryptology ePrint Archive*.

Cheng, C.-H.; Nürenberg, G.; Huang, C.-H.; and Ruess, H. 2018. Verification of binarized neural networks via interneuron factoring. In *Working Conference on Verified Software: Theories, Tools, and Experiments*, 279–290. Springer.

Cheng, C.-H.; Nürenberg, G.; and Ruess, H. 2017. Maximum resilience of artificial neural networks. In *International Symposium on Automated Technology for Verification and Analysis*, 251–268. Springer.

Croce, F.; Andriushchenko, M.; Sehwag, V.; Debenedetti, E.; Flammarion, N.; Chiang, M.; Mittal, P.; and Hein, M. 2021. RobustBench: a standardized adversarial robustness benchmark. In *Thirty-fifth Conference on Neural Information Processing Systems Datasets and Benchmarks Track*.

De Palma, A.; Bunel, R.; Dvijotham, K.; Kumar, M. P.; and Stanforth, R. 2022. IBP Regularization for Verified Adversarial Robustness via Branch-and-Bound. *arXiv preprint arXiv:2206.14772*.

Deng, J.; Dong, W.; Socher, R.; Li, L.-J.; Li, K.; and Fei-Fei, L. 2009. ImageNet: A Large-Scale Hierarchical Image Database. In *CVPR09*.

Dosovitskiy, A.; Beyer, L.; Kolesnikov, A.; Weissenborn, D.; Zhai, X.; Unterthiner, T.; Dehghani, M.; Minderer, M.; Heigold, G.; Gelly, S.; et al. 2020. An image is worth 16x16 words: Transformers for image recognition at scale. *arXiv preprint arXiv:2010.11929*.

Driscoll, M. 2020. System and method for adapting a neural network model on a hardware platform. US Patent App. 16/728,884.

Dumoulin, V.; and Visin, F. 2016. A guide to convolution arithmetic for deep learning. *arXiv preprint arXiv:1603.07285*.

Dvijotham, K.; Gowal, S.; Stanforth, R.; Arandjelovic, R.; O’Donoghue, B.; Uesato, J.; and Kohli, P. 2018. Training verified learners with learned verifiers. *arXiv preprint arXiv:1805.10265*.

Eén, N.; and Sörensson, N. 2006. Translating pseudo-boolean constraints into SAT. *Journal on Satisfiability, Boolean Modeling and Computation*, 2(1-4): 1–26.

Ehlers, R. 2017. Formal verification of piece-wise linear feed-forward neural networks. In *International Symposium on Automated Technology for Verification and Analysis*, 269–286. Springer.

Evans, R.; Bošnjak, M.; Buesing, L.; Ellis, K.; Pfau, D.; Kohli, P.; and Sergot, M. 2021. Making sense of raw input. *Artificial Intelligence*, 299: 103521.

Ferrari, C.; Muller, M. N.; Jovanovic, N.; and Vechev, M. 2022. Complete verification via multi-neuron relaxation guided branch-and-bound. *arXiv preprint arXiv:2205.00263*.

Garg, S.; Perot, V.; Limtiaco, N.; Taly, A.; Chi, E. H.; and Beutel, A. 2019. Counterfactual fairness in text classification through robustness. In *Proceedings of the 2019 AAAI/ACM Conference on AI, Ethics, and Society*, 219–226.

Goodfellow, I.; Bengio, Y.; and Courville, A. 2016. *Deep Learning*. MIT Press. <http://www.deeplearningbook.org>.

Hölldobler, S.; Manthey, N.; and Steinke, P. 2012. A compact encoding of pseudo-Boolean constraints into SAT. In *Annual Conference on Artificial Intelligence*, 107–118. Springer.

Hong, S.; Frigo, P.; Kaya, Y.; Giuffrida, C.; and Dumitras, T. 2019. Terminal brain damage: Exposing the graceless degradation in deep neural networks under hardware fault attacks. In *28th USENIX Security Symposium (USENIX Security 19)*, 497–514.

Huan, Z.; Kaidi, X.; Shiqi, W.; and Cho-Jui, H. 2022. AAAI 2022: ‘Tutorial on Neural Network Verification: Theory and Practice’. <Https://neural-network-verification.com/>.

Hubara, I.; Courbariaux, M.; Soudry, D.; El-Yaniv, R.; and Bengio, Y. 2016. Binarized neural networks. *Advances in neural information processing systems*, 29.

Ignatiev, A.; Morgado, A.; and Marques-Silva, J. 2018. PySAT: A Python Toolkit for Prototyping with SAT Oracles. In *SAT*, 428–437.

Jia, K.; and Rinard, M. 2020. Efficient exact verification of binarized neural networks. *arXiv preprint arXiv:2005.03597*.

Jia, K.; and Rinard, M. 2021a. Exploiting verified neural networks via floating point numerical error. In *International Static Analysis Symposium*, 191–205. Springer.

Jia, K.; and Rinard, M. 2021b. Verifying Low-Dimensional Input Neural Networks via Input Quantization. In *International Static Analysis Symposium*, 206–214. Springer.

Katz, G.; Barrett, C.; Dill, D. L.; Julian, K.; and Kochenderfer, M. J. 2017. Reluplex: An efficient SMT solver for verifying deep neural networks. In *International Conference on Computer Aided Verification*, 97–117. Springer.

Kingma, D. P.; and Ba, J. 2014. Adam: A method for stochastic optimization. *arXiv preprint arXiv:1412.6980*.

Kurtz, J.; and Bah, B. 2021. Efficient and Robust Mixed-Integer Optimization Methods for Training Binarized Deep Neural Networks. *arXiv preprint arXiv:2110.11382*.

Liffiton, M. H.; and Maglalang, J. C. 2012. A cardinality solver: More expressive constraints for free. In *International Conference on Theory and Applications of Satisfiability Testing*, 485–486. Springer.

Liu, Z.; Wu, B.; Luo, W.; Yang, X.; Liu, W.; and Cheng, K.-T. 2018. Bi-real net: Enhancing the performance of 1-bit cnns with improved representational capability and advanced training algorithm. In *Proceedings of the European conference on computer vision (ECCV)*, 722–737.

Lomuscio, A.; and Maganti, L. 2017. An approach to reachability analysis for feed-forward relu neural networks. *arXiv preprint arXiv:1706.07351*.

Lomuscio, A.; Qu, H.; and Raimondi, F. 2017. MCMAS: an open-source model checker for the verification of multi-agent systems. *International Journal on Software Tools for Technology Transfer*, 19(1): 9–30.

Loshchilov, I.; and Hutter, F. 2016. Sgdr: Stochastic gradient descent with warm restarts. *arXiv preprint arXiv:1608.03983*.

Madry, A.; Makelov, A.; Schmidt, L.; Tsipras, D.; and Vladu, A. 2017. Towards deep learning models resistant to adversarial attacks. *arXiv preprint arXiv:1706.06083*.

Manthey, N.; Philipp, T.; and Steinke, P. 2014. A more compact translation of pseudo-Boolean constraints into CNF such that generalized arc consistency is maintained. In *Joint German/Austrian Conference on Artificial Intelligence (Künstliche Intelligenz)*, 123–134. Springer.

Meurer, A.; Smith, C. P.; Paprocki, M.; Čertík, O.; Kirpichev, S. B.; Rocklin, M.; Kumar, A.; Ivanov, S.; Moore, J. K.; Singh, S.; Rathnayake, T.; Vig, S.; Granger, B. E.; Muller, R. P.; Bonazzi, F.; Gupta, H.; Vats, S.; Johansson, F.; Pedregosa, F.; Curry, M. J.; Terrel, A. R.; Roučka, v.; Saboo, A.; Fernando, I.; Kulal, S.; Cimrman, R.; and Scopatz, A. 2017. SymPy: symbolic computing in Python. *PeerJ Computer Science*, 3: e103.

Mirman, M.; Gehr, T.; and Vechev, M. 2018. Differentiable abstract interpretation for provably robust neural networks. In *International Conference on Machine Learning*, 3578–3586. PMLR.

Müller, M. N.; Makarchuk, G.; Singh, G.; Püschel, M.; and Vechev, M. 2022. PRIMA: general and precise neural network certification via scalable convex hull approximations. *Proceedings of the ACM on Programming Languages*, 6(POPL): 1–33.

Narodytska, N.; Kasiviswanathan, S.; Ryzhyk, L.; Sagiv, M.; and Walsh, T. 2018. Verifying properties of binarized deep neural networks. In *Proceedings of the AAAI Conference on Artificial Intelligence*, volume 32.

Narodytska, N.; Shrotri, A.; Meel, K. S.; Ignatiev, A.; and Marques-Silva, J. 2019a. Assessing heuristic machine learning explanations with model counting. In *International Conference on Theory and Applications of Satisfiability Testing*, 267–278. Springer.

Narodytska, N.; Zhang, H.; Gupta, A.; and Walsh, T. 2019b. In search for a SAT-friendly binarized neural network architecture. In *International Conference on Learning Representations*.

Paszke, A.; Gross, S.; Massa, F.; Lerer, A.; Bradbury, J.; Chanan, G.; Killeen, T.; Lin, Z.; Gimelshein, N.; Antiga, L.; et al. 2019. Pytorch: An imperative style, high-performance deep learning library. *Advances in neural information processing systems*, 32: 8026–8037.

Quine, W. V. 1952. The problem of simplifying truth functions. *The American mathematical monthly*, 59(8): 521–531.

Raghunathan, A.; Steinhardt, J.; and Liang, P. 2018. Certified defenses against adversarial examples. *arXiv preprint arXiv:1801.09344*.

Rakin, A. S.; He, Z.; and Fan, D. 2020. Tbt: Targeted neural network attack with bit trojan. In *Proceedings of the IEEE/CVF Conference on Computer Vision and Pattern Recognition*, 13198–13207.

Rastegari, M.; Ordonez, V.; Redmon, J.; and Farhadi, A. 2016. Xnor-net: Imagenet classification using binary convolutional neural networks. In *European conference on computer vision*, 525–542. Springer.

Regulation, G. D. P. 2016. Regulation EU 2016/679 of the European Parliament and of the Council of 27 April 2016. *Official Journal of the European Union*. Available at: http://ec.europa.eu/justice/data-protection/reform/files/regulation_oj_en.pdf (accessed 20 September 2017).

Roussel, O.; and Manquinho, V. 2009. Pseudo-Boolean and cardinality constraints. In *Handbook of satisfiability*, 695–733. IOS Press.

Sahoo, S. S.; Venugopalan, S.; Li, L.; Singh, R.; and Riley, P. 2020. Scaling Symbolic Methods using Gradients for Neural Model Explanation. *arXiv preprint arXiv:2006.16322*.

Sandler, M.; Howard, A.; Zhu, M.; Zhmoginov, A.; and Chen, L.-C. 2018. Mobilenetv2: Inverted residuals and linear bottlenecks. In *Proceedings of the IEEE conference on computer vision and pattern recognition*, 4510–4520.

Sanyal, A.; Kusner, M.; Gascon, A.; and Kanade, V. 2018. TAPAS: Tricks to accelerate (encrypted) prediction as a service. In *International Conference on Machine Learning*, 4490–4499. PMLR.

Shih, A.; Darwiche, A.; and Choi, A. 2019. Verifying binarized neural networks by local automaton learning. In *AAAI Spring Symposium on Verification of Neural Networks (VNN)*.

Singh, G.; Ganvir, R.; Püschel, M.; and Vechev, M. 2019a. Beyond the single neuron convex barrier for neural network certification. *Advances in Neural Information Processing Systems*, 32.

Singh, G.; Gehr, T.; Püschel, M.; and Vechev, M. 2019b. An abstract domain for certifying neural networks. *Proceedings of the ACM on Programming Languages*, 3(POPL): 1–30.

Sun, B.; Sun, J.; Dai, T.; and Zhang, L. 2021. Probabilistic verification of neural networks against group fairness. In *International Symposium on Formal Methods*, 83–102. Springer.

Tjandraatmadja, C.; Anderson, R.; Huchette, J.; Ma, W.; PATEL, K. K.; and Vielma, J. P. 2020. The convex relaxation barrier, revisited: Tightened single-neuron relaxations for neural network verification. *Advances in Neural Information Processing Systems*, 33: 21675–21686.

Tjeng, V.; Xiao, K.; and Tedrake, R. 2019. Evaluating robustness of neural networks with mixed integer programming. *ICLR*.

Vaswani, A.; Shazeer, N.; Parmar, N.; Uszkoreit, J.; Jones, L.; Gomez, A. N.; Kaiser, Ł.; and Polosukhin, I. 2017. Attention is all you need. In *Advances in neural information processing systems*, 5998–6008.

Wang, S.; Zhang, H.; Xu, K.; Lin, X.; Jana, S.; Hsieh, C.-J.; and Kolter, J. Z. 2021a. Beta-crown: Efficient bound propagation with per-neuron split constraints for complete and incomplete neural network verification. *arXiv preprint arXiv:2103.06624*.

Wang, Z.; Zhang, W.; Liu, N.; and Wang, J. 2021b. Scalable Rule-Based Representation Learning for Interpretable Classification. *Advances in Neural Information Processing Systems*, 34.

Wong, E.; and Kolter, Z. 2018. Provable defenses against adversarial examples via the convex outer adversarial polytope. In *International Conference on Machine Learning*, 5286–5295. PMLR.

Wong, E.; Schmidt, F. R.; Metzen, J. H.; and Kolter, J. Z. 2018. Scaling provable adversarial defenses. *arXiv preprint arXiv:1805.12514*.

Wu, H.; Barrett, C.; Sharif, M.; Narodytska, N.; and Singh, G. 2022. Scalable Verification of GNN-based Job Schedulers. *arXiv preprint arXiv:2203.03153*.

Xiao, K. Y.; Tjeng, V.; Shafiuallah, N. M. M.; and Madry, A. 2019. Training for Faster Adversarial Robustness Verification via Inducing ReLU Stability. In *International Conference on Learning Representations*.

Xu, K.; Shi, Z.; Zhang, H.; Wang, Y.; Chang, K.-W.; Huang, M.; Kailkhura, B.; Lin, X.; and Hsieh, C.-J. 2020a. Automatic Perturbation Analysis for Scalable Certified Robustness and Beyond. In Larochelle, H.; Ranzato, M.; Hadsell, R.; Balcan, M.; and Lin, H., eds., *Advances in Neural Information Processing Systems*, volume 33, 1129–1141. Curran Associates, Inc.

Xu, K.; Shi, Z.; Zhang, H.; Wang, Y.; Chang, K.-W.; Huang, M.; Kailkhura, B.; Lin, X.; and Hsieh, C.-J. 2020b. Automatic perturbation analysis for scalable certified robustness and beyond. *Advances in Neural Information Processing Systems*, 33: 1129–1141.

Yang, F.; He, K.; Yang, L.; Du, H.; Yang, J.; Yang, B.; and Sun, L. 2021. Learning Interpretable Decision Rule Sets: A Submodular Optimization Approach. *Advances in Neural Information Processing Systems*, 34.

Zhang, B.; Cai, T.; Lu, Z.; He, D.; and Wang, L. 2021a. Towards certifying l -infinity robustness using neural networks with l -inf-dist neurons. In *International Conference on Machine Learning*, 12368–12379. PMLR.

Zhang, H.; Chen, H.; Xiao, C.; Gowal, S.; Stanforth, R.; Li, B.; Boning, D.; and Hsieh, C.-J. 2019. Towards stable and efficient training of verifiably robust neural networks. *arXiv preprint arXiv:1906.06316*.

Zhang, Y.; Zhao, Z.; Chen, G.; Song, F.; and Chen, T. 2021b. BDD4BNN: a BDD-based quantitative analysis framework for binarized neural networks. In *International Conference on Computer Aided Verification*, 175–200. Springer.

A Definitions and notations

First, we introduce the definitions of a DNN verifiably robust, soundness and completeness verification methods, and the verified accuracy.

We define a dataset \mathcal{D} and the subsets $\mathcal{D}_1, \mathcal{D}_2$ of \mathcal{D} such that $\mathcal{D}_1 \cup \mathcal{D}_2 = \mathcal{D}$ and $\mathcal{D}_1 \cap \mathcal{D}_2 = \emptyset$. We define F_θ as the DNN with parameters θ and \mathcal{P} as the property. We consider that for all inputs from \mathcal{D}_1 we have that \mathcal{P} holds, whereas for all inputs from \mathcal{D}_2 , \mathcal{P} does not hold. In our case, we only consider the verifiably robust DNN as the property \mathcal{P} , which is defined as follows.

Definition: Verifiably robust property. *Given an input x and its label y from the dataset \mathcal{D} , a norm p , a DNN F_θ is **verifiably robust** on input x at the given noise level $\epsilon > 0$ if for $\|x - x'\|_p < \epsilon$ one has $F_\theta(x) = F_\theta(x') = y$ for all x' .*

Definition: Sound, complete, verifiable, certification, robustness methods and accuracies. *Given a dataset \mathcal{D} and a DNN F_θ , the **natural accuracy** is the ratio of data $(x, y) \in \mathcal{D}$ such that $F_\theta(x) = y$. For a method \mathcal{M} and a property \mathcal{P} , we define various type of methods as follows:*

- if for all inputs in \mathcal{D}_2 , \mathcal{M} states that \mathcal{P} does not hold then \mathcal{M} is **sound**.
- if for all inputs in \mathcal{D}_1 , \mathcal{M} states that \mathcal{P} does hold then \mathcal{M} is **complete**.
- if there exists an input in \mathcal{D}_2 such that \mathcal{M} states that \mathcal{P} holds or \mathcal{M} never halts, then \mathcal{M} is **unsound**.

Table 9: Examples of inequality conversion into SAT formulas according to different methodologies. The first row presents one inequality example containing 3 natural variables (x_1, x_2, x_3). The corresponding output SAT encodings are given for 5 different published methods (Abío et al. 2011; Hölldobler, Manthey, and Steinke 2012; Eén and Sörensson 2006; Manthey, Philipp, and Steinke 2014). The SAT equation outputs include many literals and clauses, adding complexity to the problem. Moreover, there is no straightforward relationship between the SAT literals l_i and the variables x_i , or between the clauses and the inequality coefficients.

SAT encoding and source	Inequality to convert into SAT Formulas: $x_1 - 2x_2 + 3x_3 \leq 3$
Encoding 1 (Abío et al. 2011)	$(l_4) \wedge (\overline{l_1} \vee l_2 \vee \overline{l_5}) \wedge (l_5 \vee \overline{l_3} \vee \overline{l_6}) \wedge (l_6)$
Encoding 2 (Hölldobler, Manthey, and Steinke 2012)	$(\overline{l_4} \vee l_9) \wedge (\overline{l_5} \vee l_{10}) \wedge (\overline{l_6} \vee l_{11})$ $\wedge (\overline{l_7} \vee l_{12}) \wedge (\overline{l_8} \vee l_{13}) \wedge (\overline{l_9} \vee l_{14}) \wedge (\overline{l_{10}} \vee l_{15}) \wedge (\overline{l_{11}} \vee l_{16})$ $\wedge (\overline{l_{12}} \vee l_{17}) \wedge (\overline{l_{13}} \vee l_{18}) \wedge$ $(\overline{l_3} \vee l_4) \wedge (\overline{l_3} \vee l_5) \wedge (\overline{l_3} \vee l_6) \wedge$ $(l_2 \vee l_9) \wedge (l_2 \vee l_{10}) \wedge (\overline{l_1} \vee l_{14}) \wedge (\overline{l_4} \vee l_2 \vee l_{11}) \wedge$ $(\overline{l_5} \vee l_2 \vee l_{12}) \wedge (\overline{l_6} \vee l_2 \vee l_{13}) \wedge (\overline{l_9} \vee \overline{l_1} \vee l_{15}) \wedge$ $(\overline{l_{10}} \vee \overline{l_1} \vee l_{16}) \wedge (\overline{l_1} \vee l_1 \vee l_{17}) \wedge (\overline{l_{12}} \vee \overline{l_1} \vee l_{18}) \wedge (\overline{l_7}) \wedge$ $(\overline{l_8}) \wedge (\overline{l_7} \vee l_2) \wedge (\overline{l_{13}} \vee \overline{l_1})$
Encoding 3 (Eén and Sörensson 2006)	$(l_5 \vee \overline{l_3} \vee l_2) \wedge (l_7 \vee \overline{l_3} \vee \overline{l_1}) \wedge (\overline{l_8} \vee \overline{l_3}) \wedge (\overline{l_8} \vee l_2) \wedge (l_6 \vee l_8 \vee \overline{l_7}) \wedge (l_4 \vee \overline{l_6} \vee \overline{l_5}) \wedge (\overline{l_4})$
Encoding 4 (Eén and Sörensson 2006)	$(\overline{l_3} \vee \overline{l_1} \vee \overline{l_4}) \wedge (l_3 \vee l_1 \vee \overline{l_4}) \wedge (\overline{l_3} \vee l_1 \vee l_4) \wedge (l_3 \vee \overline{l_1} \vee l_4) \wedge (l_3 \vee \overline{l_5}) \wedge$ $(l_1 \vee \overline{l_5}) \wedge (\overline{l_3} \vee \overline{l_1} \vee l_5) \wedge (l_2 \vee \overline{l_2} \vee l_5 \vee \overline{l_6}) \wedge (l_3 \vee l_2 \vee \overline{l_5} \vee \overline{l_6}) \wedge$ $(\overline{l_3} \vee \overline{l_2} \vee \overline{l_5} \vee l_6) \wedge (\overline{l_3} \vee l_2 \vee \overline{l_5} \vee l_6) \wedge (\overline{l_3} \vee \overline{l_2} \vee \overline{l_5} \vee \overline{l_6}) \wedge$ $\wedge (\overline{l_3} \vee \overline{l_2} \vee l_5 \vee l_6) \wedge (l_3 \vee \overline{l_2} \vee \overline{l_5} \vee l_6) \wedge (\overline{l_2} \vee l_5 \vee \overline{l_7}) \wedge (l_3 \vee l_5 \vee \overline{l_7}) \wedge (l_3 \vee \overline{l_2} \vee \overline{l_7})$ $\wedge (l_2 \vee \overline{l_5} \vee l_7) \wedge (\overline{l_3} \vee \overline{l_5} \vee l_7) \wedge (\overline{l_3} \vee l_2 \vee l_7) \wedge (\overline{l_7} \vee \overline{l_6} \vee l_3) \wedge$ $(\overline{l_7} \vee \overline{l_6} \vee \overline{l_2}) \wedge (\overline{l_7} \vee \overline{l_6} \vee l_5) \wedge (l_7 \vee l_6 \vee \overline{l_3}) \wedge (l_7 \vee l_6 \vee l_2) \wedge (l_7 \vee l_6 \vee \overline{l_5}) \wedge (\overline{l_7} \vee \overline{l_6})$
Encoding 5 (Manthey, Philipp, and Steinke 2014)	$(l_4) \wedge (\overline{l_3} \vee l_5) \wedge (\overline{l_1} \vee l_5) \wedge (\overline{l_3} \vee \overline{l_1} \vee l_6) \wedge (\overline{l_3} \vee l_7) \wedge (l_2 \vee l_7) \wedge (\overline{l_3} \vee l_2 \vee l_8) \wedge (\overline{l_7} \vee l_9) \wedge$ $(\overline{l_8} \vee l_{10}) \wedge (\overline{l_6} \vee l_9) \wedge (\overline{l_7} \vee \overline{l_6} \vee l_{10}) \wedge (\overline{l_8} \vee \overline{l_6} \vee l_{11}) \wedge (\overline{l_1} \vee l_1)$

- if there exist an input in \mathcal{D}_1 such that \mathcal{M} states that \mathcal{P} does not hold or \mathcal{M} never halts, \mathcal{M} is **incomplete**.
- a **verifiable method** \mathcal{M}_V is a sound and complete method. The **verified accuracy** is the ratio of data $(x, y) \in \mathcal{D}$ such that $F_\theta(x) = y$ and \mathcal{M}_V states that \mathcal{P} holds.
- a **certification method** \mathcal{M}_C is a sound and incomplete method. The **certification accuracy** is the ratio of data $(x, y) \in \mathcal{D}$ such that $F_\theta(x) = y$ and \mathcal{M}_C states that \mathcal{P} holds.
- a **robust method** \mathcal{M}_R is an unsound method. The **robust accuracy** is the ratio of data $(x, y) \in \mathcal{D}$ such that $F_\theta(x) = y$ and \mathcal{M}_R states that \mathcal{P} holds.

We also define the method \mathcal{M} of verification of the property \mathcal{P} on F_θ for the dataset \mathcal{D} . \mathcal{M} can use an exact solver (like a SAT solver), a probabilistic solver, or no solver at all (as in the case of PGD attacks (Madry et al. 2017)). \mathcal{M} has three different possible outcomes: \mathcal{P} holds, \mathcal{P} does not hold, or \mathcal{M} never halts. When using solvers and if the method never halts, the solvers will output a timeout.

Verifiable methods can be mainly divided into SMT-based methods (Katz et al. 2017), Mixed-Integer Linear Programming MILP-based methods (Xiao et al. 2019), or SAT-based methods. There are few works and the gap between natural and verified accuracy remains important. Certification methods try to fill this gap by proposing a trade-off between security and performance. In contrary, the literature concerning robustness methods is large: we refer to (Croce et al. 2021; Carlini et al. 2019) that compares and benchmarks these methods.

In this work, F_θ is the TTnet model, \mathcal{D} is either MNIST or CIFAR-10 and we only consider the infinity norm ($p = \infty$).

Furthermore, the noise level ϵ is $\{0.1, 0.3\}$ for MNIST and $\{2/255, 8/255\}$ for CIFAR-10. Our method \mathcal{M}_V is verified as it is sound and complete. We use the exact and generic SAT solver MiniCard (Liffiton and Maglalang 2012), in contrast to a probabilistic one as in (Zhang et al. 2021b) or a handcrafted one as in (Jia and Rinard 2020)).

B Examples of pseudo-Boolean constraint encoding

Table 9 presents a few examples of pseudo-Boolean constraint encoding.

C Model details

C.1 Overall architecture

In this study, we considered the three architectures shown in Table 10. All the paddings are set to 0.

C.2 First layer: pre-processing layer

Before applying the batch normalisation and the step function, we quantify the inputs as $x^q = \lfloor \frac{x}{q} \rfloor \cdot s$ where x is the real-valued input, x^q is the quantized input to be fed into the TTnet and s is the quantization step size which can be set to $s = 1/255$ to emulate 8-bit fixed-point values, or 2ϵ for adversarial training with a l_∞ disturbance limit of ϵ . (Jia and Rinard 2020)

C.3 Last layer: linear classifier

Last layer. The last linear layer is composed of a linear layer and a batch normalisation. The weights of the linear layer can be natural instead of binary but this leads to a large increase in the size of the SAT formulas.

Table 10: Different studied model architectures with TTnet.

Dataset	Name	Layers	# of blocks	Filters sizes	Amplification	Kernels	Groups	Strides	Features	Parameters	FLOPS	Patch size
MNIST	Model A(6,6)	4	2	60-48-384-48	1.25-8	3-1-2-1	1-1-24-24	3-1-2-1	768	15488	0.63 m	(6,6)
	Model B(7,7)	4	2	60-48-384-48	1.25-8	3-1-3-1	1-1-48-48	2-1-2-1	2352	30780	0.77 m	(7,7)
	Model C(7,7)	4	2	144-48-384-48	3-8	3-1-3-1	1-1-48-48	2-1-1-1	8112	86580	0.98 m	(7,7)
CIFAR 10	Model A(6,6)	4	2	60-48-384-48	1.25-8	3-1-2-1	3-3-24-24	3-1-2-1	1200	17890	0.89 m	(6,6)
	Model B(7,7)	4	2	60-48-384-48	1.25-8	3-1-3-1	3-3-48-48	2-1-2-1	2352	30780	0.87 m	(7,7)
	Model C(7,7)	4	2	144-48-384-48	3-8	3-1-3-1	1-1-48-48	2-1-1-1	8112	86580	1.12 m	(7,7)

Natural features. We may also increase the amount of information held by the vector of features V by accepting natural values. Coming back to our Example 1 for Section 3.1, we can see the output $y = [0, -5, 3, -2, 1, -4, 4, -1, 10, 5, 13, 8, 11, 6, 14, 9]$ as $y = -5 \times [0, 1, 0, 0, 0, 0, 0, 0, 0, 0, 0, 0, 0, 0, 0, 0] + 3 \times [0, 0, 1, 0, 0, 0, 0, 0, 0, 0, 0, 0, 0, 0, 0, 0] + \dots + 9 \times [0, 0, 0, 0, 0, 0, 0, 0, 0, 0, 0, 0, 0, 0, 0, 1]$. Therefore, each of these coefficients can have an associated SAT expression of its own.

For the sake of natural accuracy performance, as in (Evans et al. 2021), it is advisable to encode features and weights on 8 bits. Results for features and weights encoded on 8 bits are given in Appendix F. However, the results in this paper are given for binary features and weights.

As we trained the TTnet with a final linear layer then a batch normalisation, we encoded the last layer for the label i as follows:

$$y_i = \sum_{k=1}^{|V|} w_{k,i} V_k + b_i$$

and

$$\begin{aligned} y_i^{BN} &= \text{BatchNorm}(y_i) = \gamma \cdot \frac{y_i - \mathbb{E}(y_i)}{\sqrt{\text{Var}[y_i] + \epsilon}} + \beta \\ &= \frac{\sum_{k=1}^{|V|} \gamma w_{k,i} V_k + \gamma b_i - \mathbb{E}(y_i)}{\sqrt{\text{Var}[x] + \epsilon}} + \beta \end{aligned}$$

with $\epsilon = 1e-5$ and \cdot denotes element-wise multiplication. We can rewrite the equality as:

$$\begin{aligned} y_i^{BN} &= \sum_{k=1}^{|V|} \tilde{w}_{k,i} V_k + \tilde{b}_i \\ \tilde{w}_{k,i} &= \lfloor \frac{\gamma w_{k,i}}{\sqrt{\text{Var}[y_i] + \epsilon}} \rfloor \\ \tilde{b}_i &= \frac{\gamma b_i - \mathbb{E}(y_i)}{\sqrt{\text{Var}[y_i] + \epsilon}} + \beta \end{aligned}$$

To facilitate the SAT conversion, we also restrict the variance statistics and the scale parameter γ in `BatchNorm()` of the last layer to be scalars computed on the whole feature map rather than per-channel statistics. Before rounding, we multiply $\tilde{w}_{k,i}$ and \tilde{b}_i by 100 in order to keep some details contained in the floating points. This inequality is en-

coded with the project (Ignatiev, Morgado, and Marques-Silva 2018). The overall project is based on Sympy (Meurer et al. 2017).

D Training and Pre/Post-tuning details

Experimental environment. The project was implemented with Python and the library PyTorch (Paszke et al. 2019).

Training method. We built our training method on top of (Jia and Rinard 2020) project and we refer to their notations for this section. We trained the networks using the Adam optimizer (Kingma and Ba 2014) for 90 epochs with a mini-batch size of 128. The mean and variance statistics of batch normalization layers are recomputed on the whole training set after training finishes.

Learning rate is 0.0005. We use Projected Gradient Descent (PGD (Madry et al. 2017)) with adaptive gradient cancelling to train robust networks, where the perturbation bound ϵ is increased linearly from 0 to the desired value in the first 50 epochs and the number of PGD iteration steps grows linearly from 0 to 10 in the first 23 epochs.

The parameter α in adaptive gradient cancelling is chosen to maximize the PGD attack success rate evaluated on 40 minibatches of training data sampled at the first epoch. Candidate values of α are between 0.6 to 3.0 with a step of 0.4. Note that α is a global parameter shared by all neurons. We do not use any data augmentation techniques for training. Due to limited computing resources and significant differences between the settings we considered, data in this paper are reported based on one evaluation run.

Weights initialization. Weights for the final connected layers are initialized from a Gaussian distribution with standard deviation 0.01, and the mask weights in BinMask are enforced to be positive by taking the absolute value during initialization.

Post-tuning parameters. We use a proportion ratio of 0.1 and a probability $p = 0.05$ for MNIST low noise, we double it for high noise and a proportion ratio of 0.05 and a probability $p = 0.01$ for CIFAR-10 low noise and we double it for high noise.

Other hyperparameters. The input quantization step s is set to be $0.61 = 0.3 \times 2 + 0.01$ for training on the MNIST dataset, and $0.064 \approx 16.3/255$ for CIFAR-10, which are chosen to be slightly greater than twice the largest perturbation bound we consider for each dataset. Except for CIFAR-10 for which we double the training noise, the training noise

level is equal to the testing noise level. The CBD loss is applied on MNIST high noise only and ν is set to be $5e-4$, 0 otherwise. We apply a weight decay of $1e-7$ on the binarized mask weight of BinMask. We use the encoding proposed in (Abío et al. 2011) for the linear regression encoding into SAT. In Table 7, we use Model C(7,7) except for the high noise model with CIFAR-10, we use Model A.

Training/testing comparison. We provide in Table 11 a comparison of the training/testing time for TTnet, BNN, and DCNN.

Table 11: Training/testing time and FLOPS comparison for MNIST.

	TTnet (n=9)	TTnet (n=27)	BNN	DCNN
Training time (on GPU in sec)	3.4×10^3	3.6×10^3	4.0×10^3	2.7×10^3
Testing time (on GPU in sec)	0.8	0.8	0.8	0.8

E Natural accuracy for ImageNET

Training details. We train the networks using the SGD optimizer for 500 epochs with a minibatch size of 128. Learning rate is 0.001, the loss is cross entropy. We use SGD momentum is 0.9 and the weight decay is 5e-4. Finally the learning rate scheduler cosine annealing (Loshchilov and Hutter 2016) with a maximum number of iterations 200. We use random crop function and horizontal flip as data augmentation techniques for training. Due to limited computing resources and significant differences between the settings we considered, data in this paper are reported based on one evaluation run.

Multi-head CNN layers. First, we add multi-head CNN layers into TTnet. Figure 3 shows the structure of the multi-head CNN layers used. With the aim to increase the learning capacity of TTnet while still maintaining a small look-up table, it makes perfect sense that we want some LTT blocks to see deeply between channels but have small kernel size (called deep-small LTT blocks), but also want some LTT blocks that have larger kernel size but shallow between channels (called shallow-big LTT block).

Residual connection. We also stabilise the training by concatenating the input. In the case of stride 2, we apply an average pooling and reuse the DSS activation function.

Shuffle operation and second stage LTT block. Finally, we shuffle the channels in order to set side by side the channels from the deep-small LTT block, followed by the shallow-small LTT block, and then the residual connection. Then we add a second LTT block that takes the three channels as input and outputs a value.

F Ablation study

F.1 Amplification layer study for natural accuracy

From a practical standpoint, using eight filters in layer one and one filter in layer two drastically improves the learning capacity of the TTnet and therefore the natural accuracy

as well. This observation is consistent with other published studies (Sandler et al. 2018). We computed the natural accuracy for two models (model A(6,6) and model B(7,7)), for three types of amplifications (no amplification, $\times 4$, $\times 8$) and high noise training (see Table 10 in Appendix C.1 for more details). Results are presented in Table 12. We confirm that in all cases, adding an amplification layer significantly improves the resulting natural accuracy.

Table 12: Effect of amplification layer on TTnet natural accuracy. Natural accuracy was examined for three different types of amplification configuration, for CIFAR-10 and MNIST, in the case of training with high noise.

Dataset	Noise Training	Amplification	Natural accuracy	
			Model A (6,6)	Model B (7,7)
MNIST	0.4	None	82.63%	92.42%
		$\times 4$	85.67%	94.19%
		$\times 8$	87.59%	95.77%
CIFAR-10	16/255	None	22.40%	28.05%
		$\times 4$	27.86%	37.29%
		$\times 8$	32.19%	47.12%

F.2 Ablation study for verified accuracy

For the study, we tested the first 1K samples of the dataset for Model A (6,6), Model B (7,7) and Model C (7,7) with and without filtering. We reported the natural accuracy, the verified accuracy, the total time to compute, the number of clauses and variables. We do not report the number of timeouts as they are all 0. The results were computed on another computer than the one used for Table 7. We took the measures for different:

- **Size of the model.** We mainly use the two models Model A (6,6) and Model B (7,7) as they have two different group value g ($g = 2$ for Model A (6,6) and $g = 1$ for Model B (7,7)). Table 13 compares the three models Model A (6,6) Model B (7,7) and Model C (7,7).
- **Dataset.** We use MNIST and CIFAR-10
- **Training noise level.**
- **Testing noise level.**
- **Loss coefficient as introduced in (Jia and Rinard 2020).**
- **Amplification Layer.** Two amplifications possible.
- **Final Layer.** Two possibilities: with binary (Bin) or ternary (Ter) weights.

Results are presented in Table 13, Table 14 and Table 15. First, we saw that MNIST and CIFAR-10 can be scaled to our two models for low and high noise. Then, we observe that the loss coefficient has little impact on the performances. We can highlight that the training noise level has an important impact on the verification accuracy and the time computation. We can observe that most of the time the filtering leads to a better verified accuracy and sometimes to a better natural accuracy.

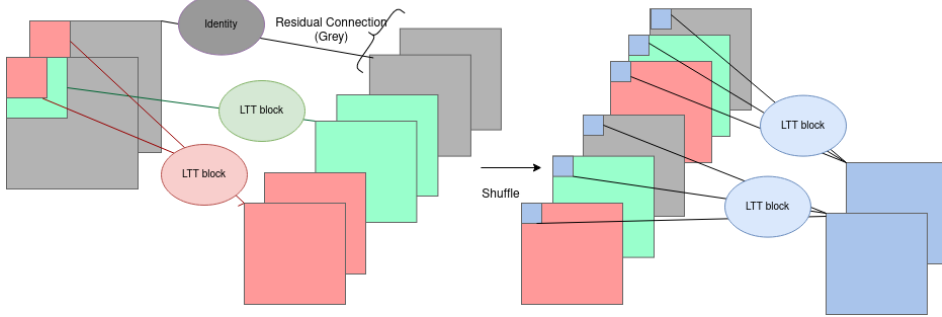


Figure 3: Multi-head CNN layers, with green layers as output from shallow-big LTT block, red as output from the deep-small LTT block and grey from the residual connection.

Table 13: Results for the three models of TTnet.

Dataset (noise)	Complete Method	Accuracy	Verification time (s)	Timeout
		Verified	Natural	
MNIST ($\epsilon_{test} = 0.1$)	TTnet Model A(6,6)	84.8%	94.3%	0.073
	TTnet Model B(7,7)	94.26%	97.70%	0.3724
	TTnet Model C(7,7)	97.12%	98.33%	0.3743
MNIST ($\epsilon_{test} = 0.3$)	TTnet Model A(6,6)	66.5%	91.2%	0.147
	TTnet Model B(7,7)	80.36%	96.73%	0.5722
	TTnet Model C(7,7)	86.24%	97.43%	0.5586
CIFAR-10 ($\epsilon_{test} = 2/255$)	TTnet Model A(6,6)	31.6%	43.1%	0.217
	TTnet Model B(7,7)	33.04 %	40.62%	0.7782
	TTnet Model C(7,7)	34.32%	49.23 %	0.2886
CIFAR-10 ($\epsilon_{test} = 8/255$)	TTnet Model A(6,6)	23.08%	31.13%	0.3887
	TTnet Model B(7,7)	22.6 %	29.4%	0.193
	TTnet Model C(7,7)	21.4%	30.4 %	0.210

E.3 Comparisons with other methods

Comparison with MIP methods. As presented in Table 16, we could demonstrate that TTnet verified accuracy is higher than that of the real value-based models in all MNIST cases. We also show that, with the general SAT solver Mini-Card, we experience a resolution time of one to two orders of magnitude faster than the real-valued models. Moreover, TTNet presents no timeout: it always returns an answer whereas it is not the case for (Xiao et al. 2019; Ferrari et al. 2022; De Palma et al. 2022), which represents another competitive advantage.

Comparison with incomplete methods. We extend the comparison to more recent works: incomplete methods that used solvers (Müller et al. 2022; Wang et al. 2021a; Singh et al. 2019b,a; Tjandraatmadja et al. 2020). We emphasize that these works are incomplete: they do not provide proof that an image correctly predicted has no adversarial attack (see Appendix A for definitions). We give in Table 17 the results for MNIST and CIFAR-10. We decided not to compare with incomplete methods that does not used solvers (Xu et al. 2020b; Zhang et al. 2021a, 2019) as, in addition to not being complete, they are specific for one property: adversarial robustness.

G Glossary

Notations glossary:

- Bin : Heaviside step function defined as $Bin(x) = \frac{1}{2} + \frac{sgn(x)}{2}$ with $x \in \mathbb{R}$
- c : number of input channels
- $c_j = l_1 \wedge \dots \wedge l_k$: conjunction j with $j \in \mathbb{N}$
- $d_j = l_1 \vee \dots \vee l_k$: disjunction j with $j \in \mathbb{N}$
- f : filter number
- g : group parameter
- k : kernel size
- l_i : literal i , $l_i = x_i$ or $l_i = \bar{x}_i$ with $i \in \mathbb{N}$
- l_∞ -norm: infinite norm
- n : number of inputs of 2D-CNN corresponding of pixel size of an input patch, $n = \frac{k^2 c}{g}$
- p : padding parameter
- $prec$: precondition on inputs (in the case of robustness, the ϵ -ball, which is concretely in Figure 4 the first U_1)
- $prop$: property on outputs. In our case, the property is that the prediction should not change under the perturbation. In Figure 4, \overline{prop} is "Class 1 higher than Class 0 and Class 1 higher than Class 2" for one of the SAT equation.
- $r_{i,j} = y_i - y_j > 0$: reified cardinality
- s : stride parameter
- sgn : sign function
- U : "Unknown" (undetermined if 0 or 1). Literal l in SAT equation.
- V : vector of features obtained in the penultimate layer after the flatten operation but before the final classification layer.
- x_i : Boolean variable i with $i \in \mathbb{N}$
- \bar{x}_i : complement of Boolean variable x_i with $i \in \mathbb{N}$
- (x_1, \dots, x_n) : set of n Boolean variables with $n \in \mathbb{N}$
- Φ : Boolean expression

Table 14: Results of TTnet in the untargeted attack set-up for MNIST

Model	Noise train	Noise test	Loss type	Amplification	Final Linear	Natural Accuracy	Verified accuracy	Verification time (s)		Timeout		#cls/#vars	
								Normal	Filtered	Normal	Filtered	Normal	Filtered
Model A (6,6)	0	0.3	0	Small	Bin	909	-	226	-	0.183	-	0	-
					Bin	936	908	169	161	0.239	0.268	0	2771/795
	0.1	0.1	0	Normal	Bin	943	937	848	665	0.073	0.128	0	3209/871
					Bin	906	902	674	648	0.139	0.207	0	2974/838
	0.3	0.3	0	Normal	Bin	906	902	674	648	0.139	0.207	0	456/199
					Bin	912	866	665	637	0.147	0.217	0	442/195
	0.4	0.3	0	Small	Bin	819	-	670	-	0.114	-	0	977/397
					Bin	859	-	676	-	0.127	-	0	1091/425
			1	Normal	Bin	889	-	651	-	0.146	-	0	1239/467
					Bin	886	881	677	680	0.117	0.245	0	1059/421
Model B (7,7)	0	0.3	0	Normal	Ter	930	-	641	-	0.324	-	0	4016/1887
					Ter	974	-	111	-	0.716	-	0	9879/2637
	0.1	0.1	0	Normal	Bin	976	978	944	947 (low)	0.302	0.494	0	1137/459
					Bin	977	977	946 (low)	946 (low)	0.491	0	0	1138/459
	0.3	0.3	0	Normal	Bin	957	953	771	776	0.463	0.634	0	4047/1250
					Bin	965	964	774	778 (high)	0.485	0.634	0	3834/1206
	0.4	0.3	0	Normal	Bin	951	-	790	-	0.423	-	0	3163/1039
					Bin	957	-	808	-	0.446	-	0	-
			1	Normal	Bin	954	931	808	781	0.436	0.590	0	3117/1062
					Ter	974	-	723	-	10.44	-	0	2816/980

Table 15: Results of TTnet in the untargeted attack set-up for CIFAR-10

Model	Noise train	Noise test	Loss type	Amplification	Final Linear	Natural Accuracy	Verified accuracy	Verification time (s)		Timeout		#cls/#vars	
								Normal	Filtered	Normal	Filtered	Normal	Filtered
Model A (6,6)	0	8/255	0	Small	Bin	448	-	20	-	0.254	-	9722/1610	-
					Bin	456	-	18	-	0.266	-	10859/1555	-
	2/255	2/255	0	Normal	Bin	460	456	328	330 (light)	0.105	0.208	661/258	639/250
					Bin	463	463	299	299 (strong)	0.200	0.200	584/233	-
			3	Normal	Bin	463	446	300	288	01:45	03:25	696/273	675/269
	2.2/255	2.2/255	0	Normal	Bin	458	431	305	316	0.106	0.217	730/279	676/257
			0	Small	Bin	348	248	190	185	0.090	0.239	1349/395	1273/390
			1	Normal	Bin	357	357	196	229 (light)	0.109	0.208	2269/509	2246/508
	8/255	8/255	1	Normal	Bin	368	347	173	231 (Strong)	0.213	0.213	2176/507	-
			3	Normal	Bin	358	299	178	186	0.110	0.223	1890/494	1519/464
			3	Normal	Bin	358	299	178	192	0.113	0.200	2337/557	2031/538
Model B (7,7)	16/255	8/255	0	Small	Bin	232	-	135	-	0.061	-	1148/368	-
					Bin	329	-	219	-	0.092	-	1342/425	-
			1	Normal	Bin	344	-	194	-	0.095	-	1339/413	-
	16.7/255	8/255	3	Normal	Bin	334	334	194	193	0.093	0.206	1473/461	1273/428
			0	Normal	Ter	390	-	139	-	0.104	-	3119/1302	-
			0	Normal	Bin	347	332	201	244	0.998	0.199	1379/451	1300/440
	2/255	8/255	0	Small	Bin	506	-	15	-	0.703	-	26183/3545	-
			0	Normal	Bin	539	-	10	-	0.640	-	23777/3874	-
			0	Normal	Bin	458	-	290	-	0.158	-	1327/452	-
	16/255	8/255	0	Normal	Bin	380	-	153	-	0.172	-	4099/730	-
			0	Small	Bin	294	-	226	-	0.193	-	3595/813	-
			0	Normal	Bin	366	-	214	-	0.205	-	4666/941	-

Acronyms glossary:

- **BNN:** Binary Neural Network
- **CNF:** conjunctive Normal Form. $\Phi = (d_1 \wedge \dots \wedge d_m)$ with $m \in \mathbb{N}$
- **DCNN:** Deep Convolutional Neural Network
- **DNF:** disjunctive Normal Form. $\Phi = (c_1 \vee \dots \vee c_m)$ with $m \in \mathbb{N}$
- **DNN:** Deep Neural Network
- **LTT:** Learning Truth Table
- **MIP:** Mixed Integer Programming
- **SMT:** Satisfiability Modulo Theory
- **TTnet:** Truth Table Deep Convolutional Neural Network
- **2D-CNN:** 2-Dimensional Convolutional Neural Network, given filter f , stride s , padding p , kernel size k , number of input channels c . With $(i, j) \in \mathbb{N}^2$,

x_X the X^{th} pixel of the considered image patch, $(x_1^{(i,j)}, \dots, x_n^{(i,j)})$ the set of n pixels in the considered patch which top-left pixel is located at position (i, j) in the input image.

$$\Phi_{(f,s,p,k,c)} : \mathbb{R}^n \rightarrow \mathbb{R}$$

$$(x_1^{(i,j)}, \dots, x_n^{(i,j)}) \mapsto y_f^{(i,j)} = \Phi_f(x_1^{(i,j)}, \dots, x_n^{(i,j)})$$

In our specific case, a LTT block has the form:

$$(x_1^{(i,j)}, \dots, x_n^{(i,j)}) \mapsto y_f^{(i,j)} = \Phi_f^2(GELU(\Phi_f^1(x_1^{(i,j)}, \dots, x_n^{(i,j)})))$$

with $\Phi_{(8f,s,0,k,c)}^1 : \{0,1\}^n \rightarrow \mathbb{R}^8$ and $\Phi_{(f,1,0,1,8c)}^2 : \mathbb{R}^8 \rightarrow \{0,1\}$.

Table 16: Application of TTnet to complete adversarial robustness verification for low and high noise bounded by l_∞ . We tabulate results of verified accuracy, natural accuracy and mean verification time on MNIST and CIFAR-10 datasets in comparison to state-of-the-art MIP methods. The best verified accuracy is displayed in bold.

Dataset (noise)	Complete Method	Accuracy		Verification time (s)	Timeout
		Verified	Natural		
MNIST ($\epsilon_{test} = 0.1$)	TTnet (Xiao et al. 2019)	97.12%	98.33%	0.374	0
	(Tjeng, Xiao, and Tedrake 2019)	94.33%	98.68%	5.47	0.05%
		95.62%	98.11%	3.52	0
MNIST ($\epsilon_{test} = 0.3$)	TTnet (Xiao et al. 2019)	86.24%	97.43 %	0.559	0
	(Tjeng, Xiao, and Tedrake 2019)	80.68%	97.33%	7.12	1.02%
	(Ferrari et al. 2022)*	74.21%	86.60%	5.13	0
CIFAR-10 ($\epsilon_{test} = 2/255$)	TTnet (Xiao et al. 2019)	34.32%	49.23%	0.2886	0
	(De Palma et al. 2022)	45.93%	61.12%	66.08	1.86%
	(Ferrari et al. 2022)*	61.97%	78.19%	113.42	5.70%
CIFAR-10 ($\epsilon_{test} = 8/255$)	TTnet (De Palma et al. 2022)	51.5%	63.1%	37.0	-
	(Xiao et al. 2019)	23.08%	31.13%	0.3887	0
		27.87%	51.43%	237.24	12.55%
		20.27%	40.45%	60.67	2.47%

* results given on the first 1K images of the test set.

H Pseudocode for TTnet core procedure

We provide here the core procedure for the conversion of TTnet into SAT, see Algorithms 1 and 2. The first algorithm 1 allows to convert a LTT block of a TT layer into a SAT function (CNF or DNF). The second algorithm 2 allows to compute and save the input/output relation of a LTT block for all input possibilities, in order to formally verify the LTT block according the procedure explained in Figure 4.

Algorithm 1: Convert an LTT block of TTnet into a SAT equation (CNF and DNF)

```

1: procedure LTT_TO_SAT(LTT block function  $f_{LTT}$ , kernel size  $k$ , number of elements in a group  $g$ , number of input channels  $c$ )
2:    $n = k^2c/g$ 
3:    $N = 2^n$ 
4:   Create an empty truth table  $TT$ 
5:   # build the truth table of  $f_{LTT}$ 
6:   for  $input$  in  $N$  do
7:      $input_b = input$  in base 2
8:      $input_{b,r} =$  Reshape  $input_b$  as a vector of size (g,k,k)
9:      $TT[input] = f_{LTT}(input_{b,r})$ 
10:  end for
11:  # compute its CNF and DNF
12:   $CNF =$  Quine–McCluskey( $TT$ , "CNF")
13:   $DNF =$  Quine–McCluskey( $TT$ , "DNF")
14:  return  $CNF, DNF$ 
15: end procedure

```

I Example of an adversarial sound and complete verification using SAT

Figure 4 is an example of an adversarial sound and complete verification using SAT. LTT_{B2} outputs $(\overline{U_1} \vee U_2) \wedge (U_1 \vee \overline{U_1})$ that represents the CNF relation between the unknown input U_1 and the unknown input U_2 according the filter SAT equation $x_1 \wedge \overline{x_3}$ for the input $\begin{bmatrix} x_0 & x_1 \\ x_2 & x_3 \end{bmatrix} = \begin{bmatrix} 1 & U_1 \\ 0 & 0 \end{bmatrix}$. In this

Algorithm 2: Convert the CNF of an LTT block of TTnet into a fuzzy table (inputs can be $\{0,1,U\}$) of SAT equations in CNF form

```

1: procedure CNF_DNF_TO_FT(CNF of  $f_{LTT}$ , kernel size  $k$ , number of elements in a group  $g$ , number of input channels  $c$ )
2:    $n = k^2c/g$ 
3:   Create an empty fuzzy table  $FT$ 
4:   # for all possible inputs  $\{0,1,U\}$ ,  $U = 2$ 
5:   for  $input$  in  $3^n$  do
6:      $input_t = input$  in base 3
7:     # Reduce the CNF/DNF by assigning the inputs that are not unknown
8:      $CNF' = CNF(input_t)$ 
9:      $DNF' = DNF(input_t)$ 
10:    Create a new Boolean variable  $y$ 
11:    #  $T_{cnf}$  is a function that transforms a SAT formulas into a CNF formula
12:     $FT[input] = T_{cnf}(y \vee \overline{DNF'}) \wedge T_{cnf}(CNF' \vee \overline{y})$ 
13:  end for
14:  return  $FT$ 
15: end procedure

```

example, we need to encode $U_1 = U_2$ in CNF: as all the input/output relations have been pre-computed in LTT_{B2} we simply need to give the input and save the output.

Figure 4: Example of an adversarial sound and complete verification using SAT with class 0 as the correctly predicted class for the image. After the preprocessing block, only the pixel U_1 can switch value under the norm l_∞ and noise level $\epsilon = 0.1$. As all input/outputs have been computed and stored, the first LTT block outputs 1 (which means that the perturbation does not influence the first LTT block), and the second one outputs two values: U_2 and the SAT equation that linked U_1 and U_2 . After the linear regression, two possible conditions can lead to an attack: either the attack leads to class 1 or class 2 as the final prediction. The SAT solver outputs that the first case is impossible and the second case is possible: there is an attack that leads to the prediction being switched from class 0 to class 2.

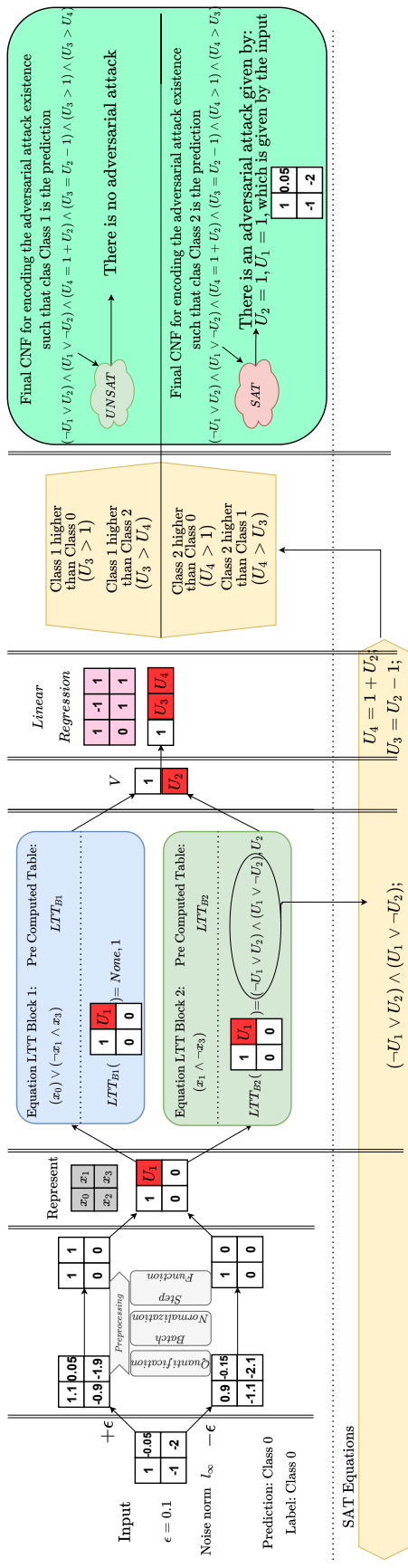


Table 17: Comparison of TTnet to incomplete adversarial robustness verification for high noise MNIST and low noise CIFAR-10 bounded by l_∞ . We tabulate results of verified accuracy and mean verification time on MNIST and CIFAR-10 datasets in comparison to state-of-the-art incomplete methods, we keep the fastest and the most accurate model for each method. The best verified accuracy is in bold and the fastest in italic. We can observe that our method has the best verified accuracy for MNIST high noise and the fastest for CIFAR-10 low noise.

Dataset (noise)	Model	CROWN/DeepPoly		kPoly		OptC2V		PRIMA		β -CROWN FSB		TTnet (Our)	
		(Singh et al. 2019b)	Verified%	(Singh et al. 2019a)	Verified%	(Tjandraatmadja et al. 2020)	Verified%	(Müller et al. 2022)	Verified%	(Wang et al. 2021a)	Verified%	Time (s)	Verified%
MNIST ($\epsilon = 0.3$)	Fastest	16.0	0.7	73.6	40	43.6	55	77.5	11	79.3	3.1	<i>86.1</i>	<i>0.56</i>
	Accurate	71.1	32	73.6	40	77.1	102	77.5	11	79.3	3.1	86.1	0.56
CIFAR-10 ($\epsilon = 2/255$)	Fastest	24.1	1	39.9	86	39.8	105	24.8	1.7	24.8	1.6	<i>35.4</i>	<i>0.29</i>
	Accurate	42.1	43	45.9	346	39.8	105	48.3	176	51.6	15.3	35.4	0.29